International Journal of Nanomedicine

Dovepress
open access to scientific and medical research

Open Access Full Text Article

ORIGINAL RESEARCH

Biodistribution, pharmacokinetics, and toxicity of dendrimer-coated iron oxide nanoparticles in BALB/c mice

This article was published in the following Dove Press journal:
International Journal of Nanomedicine

Marzieh Salimi[1,2]
Saeed Sarkar[1,2]
Samaneh Fathi[3]
Ali Mohammad Alizadeh[4]
Reza Saber[2,3]
Fatemeh Moradi[5]
Hamid Delavari[6]

[1]Department of Medical Physics and Biomedical Engineering, Tehran University of Medical Sciences, Tehran, Iran; [2]Research Center of Science and Technology in Medicine, Tehran University of Medical Sciences, Tehran, Iran; [3]Department of Medical Nanotechnology, Tehran University of Medical Sciences, Tehran, Iran; [4]Cancer Research Center, Tehran University of Medical Sciences, Tehran, Iran; [5]Department of Medical Physiology, Tehran University of Medical Sciences, Tehran, Iran; [6]Department of Materials Science and Engineering, Tarbiat Modares University, Tehran, Iran

Background: The possibility of using a specific nanoparticle in nanomedicine highly depends on its biodistribution profile and biocompatibility. Due to growing demand for iron oxide nanoparticles (IONPs) and dendrimers in biomedical applications, this study was performed to assess the biodistribution, pharmacokinetics, and toxicity of dendrimer-coated iron oxide nanoparticles (G_4@IONPs).

Materials and methods: IONPs were synthesized via co-precipitation and coated with the fourth generation (G_4) of polyamidoamine (PAMAM) dendrimer. To determine the biodistribution, 5 mg/mL G_4@IONPs suspension was intraperitoneally injected into tumor-bearing BALB/c mice, and iron levels in blood and various organs, including the lung, liver, brain, heart, tumor, and kidney, were measured by inductively coupled plasma mass spectrometry (ICP-MS) at 4, 8, 12, and 24 h after injection. Also, to investigate the toxicity of G_4@IONPs, different concentrations of G_4@IONPs were injected into BALB/c mice, and blood, renal, and hepatic factors were measured. Furthermore, histopathological staining was performed to investigate the effect of G_4@IONPs on the liver and kidney tissues.

Results: The results showed that the iron content was higher in the kidney, liver, and lung tissues 24 h after injection. Toxicity assessments revealed a significant increase in blood urea nitrogen (BUN) and direct bilirubin at the concentration of 10 mg/kg. Also, in this concentration, histopathological abnormalities were detected in liver tissue.

Conclusion: Although more systematic studies are still required, our results encouraged the future investigations of G_4@IONPs in biomedical applications.

Keywords: G_4@IONPs, biodistribution, pharmacokinetics, toxicity

Introduction

Application of nanotechnology in medicine and drug delivery is spreading fast.[1] Iron oxide nanoparticles (IONPs) are gradually being studied in different biomedical applications, including magnetic hyperthermia, targeted drug delivery, and magnetic resonance imaging (MRI) contrast agent; therefore, a comprehensive elucidation of their metabolic pathways and clearance mechanisms seems to be essential.[2] Particle size, surface charge, and coating are crucial factors affecting the biodistribution, pharmacokinetics, and also toxicity platform of IONPs.[3–5]

Weissleder et al[6] studied the biodistribution of dextran-coated superparamagnetic IONPs with an overall size of 21 nm in the rat; 25% of injected dose per gram tissue (ID/g) localized in the liver 24 h after intravenous injection, while the uptake of 80 nm IONPs in the liver was up to 83% ID only after 1 h. Furthermore, Chouly et al[3] showed

Correspondence: Marzieh Salimi
Department of Medical Physics and Biomedical Engineering, Faculty of Medicine, Tehran University of Medical Sciences, Tehran, PO Box 1417613151, Iran
Tel +98 21 66466383
Fax +98 21 66482654
Email m_salimi_rt@yahoo.com

submit your manuscript | www.dovepress.com
Dovepress
http://dx.doi.org/10.2147/IJN.S157293

similar results for biodistribution of dextran-coated IONPs with a range size of 33–90 nm. In this study, the uptake of larger nanoparticles was higher in the liver.

Surface charge is another crucial factor to determine the mechanism of cellular uptake, and the in vivo fate of nanoparticles (NPs).[7–9] Papisov et al[10] compared the positively charged and negatively charged dextran-coated IONPs biodistribution with a size of 26 nm in rats. The results clearly demonstrated that positively charged NPs mainly accumulated in the liver and spleen with a faster clearance (2 min), while the negatively charged ones were detected in the lymph nodes with a long clearance (50 min). On the other hand, the neutral surface charged IONPs had the longest circulation time, and also their uptake in the liver and spleen was much lower than positively and negatively charged ones.[3] In another study, Xiao et al[11] assessed the effect of surface charge on biodistribution of PEG-oligocholic acid based micellar NPs. The results clearly showed a high liver uptake for high positively or negatively charged NPs, while slightly negative particles had a very low liver uptake.

The coating of IONPs decreases their uptake in reticuloendothelial system (RES) organs, and makes the blood circulation time longer, which is important in biomedical applications including therapy, drug delivery, and imaging.[4] Jain et al[12] evaluated the biodistribution of 193 nm Pluronic-OA-IONPs; 55% of ID accumulated in the liver 6 h after injection, while the uptake of dextran-coated IONPs was much more in RES (>75%). In another study, IONPs with crosslinked starch and PEG coating exhibited increased half-life circulation (7–12 h).[13]

Another material which is used for surface coating of IONPs is dendrimer, which has attracted considerable attention due to its unique physicochemical properties.[14] However, the feasibility of using a special coating in biomedical applications highly depends on its biodistribution profile. Opina et al[15] investigated the gadolinium (Gd)-labeled G5 PAMAM dendrimers (G5–Gd-BnDOTA) as lymphatic imaging agents, and studied their long-term biodistribution (90-day) in mice.[15] The authors concluded that G5–Gd-BnDOTA was an appropriate agent for lymphatic imaging, but its slow clearance might prevent its subsequent clinical applications.

Few studies have investigated the biodistribution and toxicity profile of IONPs with different coatings[4,5] and dendrimers in particular. Systematic toxicity studies are required when different types of molecules or polymers are integrated into the coating layer of the IONPs.[16] Therefore, we studied the biodistribution, pharmacokinetics, and toxicity of G_4@IONPs in BALB/c mice.

Materials and methods

Materials

Ferric chloride hexahydrate ($FeCl_3 \cdot 6H_2O$, 99% w/w), ferric sulfate heptahydrate ($FeSO_4 \cdot 7H_2O$, 99% w/w), ammonia solution (NH_3, 32% v/v), hydrochloric acid (HCl, 32% v/v), 3-aminopropyltrimethoxysaline ($NH_2(CH_2)_3$-Si-$(OCH_3)_3$, APTS), methanol (99.9% v/v), ethanol (99.9% v/v), methyl acrylate (99.5% v/v), methoxy-PEG, and ethylenediamine (99% v/v) were used in the synthesis process; all materials were purchased from Sigma Aldrich (Hamburg, Germany).

Synthesis of IONPs

IONPs were prepared with the co-precipitation method. First, 0.84 g of $FeSO_4$ and 1.22 g of $FeCl_3$ were dissolved in 20 mL deionized water followed by 30 min sonication. Then, 1 mL of 2M HCl was slowly added with vigorous stirring in a nitrogen atmosphere. After 2 min, 4.6 mL ammonia was quickly added to the solution and stirring was continued for 1 min. The black precipitate of IONPs was washed five times with distilled water and ethanol through magnetic decantation.

Preparation of APTS-coated IONPs

First, 150 mL ethanol was added to 25 mL IONPs with a concentration of 5 g/L. Then, the solution was sonicated for 30 min, and 300 µL of APTS was added to the mixture after 20 min of sonication. The final solution was stirred for 15 h at room temperature and, eventually, the resultant black precipitate was washed with ethanol three times. The obtained materials were G_0 dendrimer coated IONPs (G_0@IONPs).[17]

Surface coating with PAMAM dendrimer

First, 10 mL ethanol was added to the G_0@IONPs after 30 min sonication; subsequently, methyl acrylate/methanol solution (20%, v/v) was added (50 mL) at 0°C with sonication for 1 h, followed by stirring for 48 h. After washing with methanol and magnetic decantation, ethylenediamine/methanol (50%, v/v) was added (15 mL), and the solution was sonicated for 3 h at 25°C. This procedure was repeated to complete the desired number of dendrimer generation (G_4). The product (G_4@IONPs) was washed several times with methanol and water by magnetic decantation or centrifugation.[18]

PEGylation of G_4@IONPs

Surface amino groups of dendrimer molecules were conjugated with mPEG (Mw =4,000 Da).[19,20] The mPEG mass was three times more than the mass of iron. The mPEG was

dissolved in ethanol and added to the G_4@IONPs solution followed by 18 h reflux.

Characterization

The G_4@IONPs size and morphology were assessed by transmission electron microscopy (TEM). The hydrodynamic size and surface potential were measured through dynamic light scattering (DLS) and zeta potential, respectively. Also, the crystalline phase of NPs was confirmed by x-ray diffraction (XRD, λ=0.15406 nm) and the presence of saline and PAMAM bonds on the surface of Fe_3O_4 was shown through Fourier transform infrared (FTIR) spectroscopy.

Animal experiments

The Animal Ethics Committee of Tehran University of Medical Sciences approved all animal experiments (IR.TUMS.REC.28169); Applied Research Ethics National Association guidelines were followed for the welfare of the animals. Male and Female BALB/c mice were purchased from the Animal Center of Pasture Research Center. Six- to eight-week-old male BALB/c mice weighing about 25–30 g were kept in groups of five. The groups were housed in individual cages with unlimited access to water and food. The circadian rhythm was 12 h in the light and 12 h in the dark. Male BALB/c mice were used to fulfill the toxicology studies, and female BALB/c mice were used to perform distribution and pharmacokinetics experiments.

Blood chemistry assessments

The short-term (acute) toxicity of G_4@IONPs was investigated after administration by intraperitoneal (IP) injection. Concentrations of 100, 50, 25, and 0 (control) mg/kg were administered, and there was no death or severe physical distress in test groups after injection. The mice were sacrificed 24 h after injection, and blood samples were collected in heparin-coated centrifuge tubes and centrifuged at 1,000 rpm for 2 min to acquire the plasma. Total leukocyte count (WBC), erythrocyte count (RBC), platelets (Plt), hemoglobin (Hgb), and hematocrit (Hct) were detected by an animal blood counter (Celltac; Nihon Kohden, Tokyo, Japan). Plasma alkaline phosphatase (ALP), albumin (ALB), total bilirubin, and direct bilirubin were also measured as liver function indicators (BT 3500; Autoanalyser Model Biotecnica, Rome, Italy). Renal function indicators such as BUN, creatine (Cr), and glucose (Glu) were determined using CCX System (CCX WB; Nova Biomedical, Waltham, MA, USA).[21,22]

The chronic toxicity procedure was performed similarly to the acute toxicity experiment. Concentrations of 10, 5, 1, 0.5, and 0 (control) mg/kg were injected intraperitoneally for 7 days (2 mL per injection). After the 7th day, the mice were sacrificed, and blood samples were collected to analyze the blood, renal, and hepatic factors.

Histopathology assessments

After the blood was collected, the mice were killed by cervical dislocation. The liver and kidney tissues were isolated by incision immediately after necropsy, fixed in a 10% formalin solution containing neutral phosphate-buffered saline (PBS), and stored at 4°C. The tissues were routinely processed, embedded in paraffin, sectioned at 3–5 mm, and then stained with hematoxylin and eosin (H&E) for microscopic examination.[23] Micrographs of the sections were recorded for comparison.

TUNEL staining

To assess the apoptotic effect of G_4@IONPs on cardiac tissue, terminal deoxynucleotidyl transferase-mediated dUTP nick end-labeling (TUNEL) staining was done on 10-µm-thick paraffin-embedded sections by means of the In-Situ Cell Death Detection Kit, POD (Roche Applied Science, Penzberg, Germany). Heart-muscle tissue sections were deparaffinized in xylene, rehydrated, and immersed in 3% hydrogen peroxide to block the endogenous peroxidase activity. After rinsing with PBS, the sections were kept with proteinase K solution at 37°C for 30 min to increase the staining, incubated for 60 min at 37°C with 50 µL of TUNEL reaction mixture, and then incubated for 30 min at 37°C with 50 µL of converter POD. Sections were washed in PBS, and then mounted in medium containing DAPI (4′,6-diamidino-2-phenylindole). Microscopic fields (n=5) were randomly selected and evaluated to calculate the ratio of TUNEL positive to TUNEL negative cells. For the positive control, the sections were incubated in DNase1 solution at 15°C–25°C for 10 min, and, for the negative control, enzyme solution was omitted. Finally, the sections were dehydrated again and cover-slipped as described above, and were analyzed under fluorescent microscopy.[24]

TUNEL positive cell counting

TUNEL positive cells were counted in six adjacent 100× microscopic fields, from which the number of myocytes and the ratio of apoptotic cells to normal cells were obtained. To validate the automatic counting procedure, the number of TUNEL positive cells was manually counted in five selected fields of view in a random manner under 400× magnification for each animal.

Biokinetics and tissue distribution

To study the kinetics and tissue distribution, the mice were given a 5 mg/mL G_4@IONPs suspension via IP injection.

This dose was chosen since it was low enough to be acutely nontoxic, based on the observation of the acute toxic effects, and was high enough to allow quantification of iron residue levels in organs of interest at later time points. Blood samples (~1 mL for each mouse) regained from the ocular vein were collected at predetermined time intervals (4, 8, 12, and 24 h post-injection). For the tissue distribution study, tissues (lungs, liver, brain, heart, tumor, and kidneys) were harvested at time points of 4, 8, 12, and 24 h after injection. In this experiment, saline was injected into three mice simultaneously as negative controls. All the blood and tissue samples were stored in a −80°C refrigerator for further analysis.

ICP-MS analysis

The iron analysis was based on the quantification of iron in several samples using an inductively coupled plasma-mass spectrometry (ICP-MS) method. Blood and tissue samples were thawed before analysis. About 40–80 mg of each sample was weighed, digested, and analyzed for iron content. In brief, before the elemental analysis, the blood and tissue samples of interest were digested in 5 mL nitric acid (32% v/v) overnight. Then 1 mL hydrogen peroxide (H_2O_2, 30% v/v, metal oxide semiconductor grade) was added to the solution. The solution (~1 mL) was diluted to a total volume of 2 mL with 2% nitric acid. The detection limit of iron was 0.001 ng/mL. Data are expressed as micrograms per gram (parts per million, ppm) of fresh blood or tissue normalized to the control group. To exclude the existing iron in blood and tissues, three mice were considered as a control group (saline injected). The iron content of blood and tissues of the control group was measured by ICP-MS. Finally, the measured iron content in each group was normalized to the result of the control group.

Statistical analysis

The statistical analysis was performed by one-way analysis of variance (ANOVA) test. Statistical significance was considered at $P<0.05$ in all experiments. Results are expressed as the mean ± standard deviation (n=3–5).

Results

Synthesis of G_4@IONPs

For applications of IONPs in the nanomedicine, physical and chemical characterizations are needed.[25,26] The size of G_4@IONPs was 10±4 nm according to the TEM images (Figure 1A). The hydrodynamic size of different generations of PAMAM dendrimer coated IONPs were assessed by DLS, and the results clearly showed that the hydrodynamic size of NPs increased by adding each generation of PAMAM dendrimer (Figure 1B). The surface potential of G_4@IONPs measured by zeta potential was +35 mV at pH=7 and 25°C. The hydrodynamic sizes of IONPs coated by G_1, G_2, G_3, G_4, G_4@PEG, and polydispersity of each generation are given in Table 1.

Results of XRD indicated that all diffraction peaks could be assigned to Fe_3O_4 without any impurities. The characteristic XRD pattern did not change by coating the NPs with PAMAM dendrimers (Figure 1C).[18] Furthermore, the average diffracting crystallite size of G_4@IONPs was calculated using Scherrer's equation, from the most intense peak (311),[26,27]

$$D = \frac{0.94\,\lambda}{\beta\,(2\theta)\cos\theta}$$

where D is the average crystallite size, λ is the wavelength of the incident X rays (0.154 nm), and θ is the diffraction angle (18.5°), β is the full width at half maximum in radians (0.0145), yielding a particle size of 10.6 nm, which is in close agreement with the size (10.65 nm) observed by TEM.

FTIR results related to G_1–G_4 generation of dendrimer-modified IONPs are shown in Figure 1D. The presence of the Fe_3O_4 core could be detected by the strong peaks at 570 cm^{-1}, corresponding to the intrinsic stretching vibration of the metal at the tetrahedral site (Fe tetra–O); the NH_2 group vibration is at about 3,410 cm^{-1}.[28] Moreover, the broad peak at 3,444 cm^{-1} shown the bending mode of free NH_2 groups existing at APTS.[29] The peaks of –CO–NH– bonds were detected at 1,450, 1,490, 1,570, and 1,620 cm^{-1}. The peak at 1,151 cm^{-1} demonstrated the existence of a C=O bond in ester groups, and the band at 1,480 cm^{-1} was related to the methylene group.[30] Associated with alcohols, O–H bonds were at 3,200–3,600 cm^{-1}. In fact, FTIR spectra were well-matched with the stepwise dendrimer modification procedure.

Toxicity of G_4@IONPs

Hematology and blood chemistry assessments were performed to study the toxicity effects of G_4@IONPs. In acute toxicity assessment, a significant increase in BUN levels (30 g/dL) and hyperuricemia were detected at 100 mg/kg ($P<0.05$).

Chronic exposure did not significantly change blood parameters (Figure 2A) and renal function indicators (Figure 2B) at all G_4@IONPs concentrations. There was also a non-significant increase in ALP and ALT (alanine aminotransferase) enzymes, possibly due to the transfer of oleic acid molecules from liver macrophages to hepatocytes, or the impact of G_4@IONPs injection (Figure 2C). Furthermore, direct bilirubin (an estimate of the conjugated bilirubin) increased significantly ($P<0.05$) at 10 mg/kg (0.66 g/dL versus 0.2 g/dL in the control group).

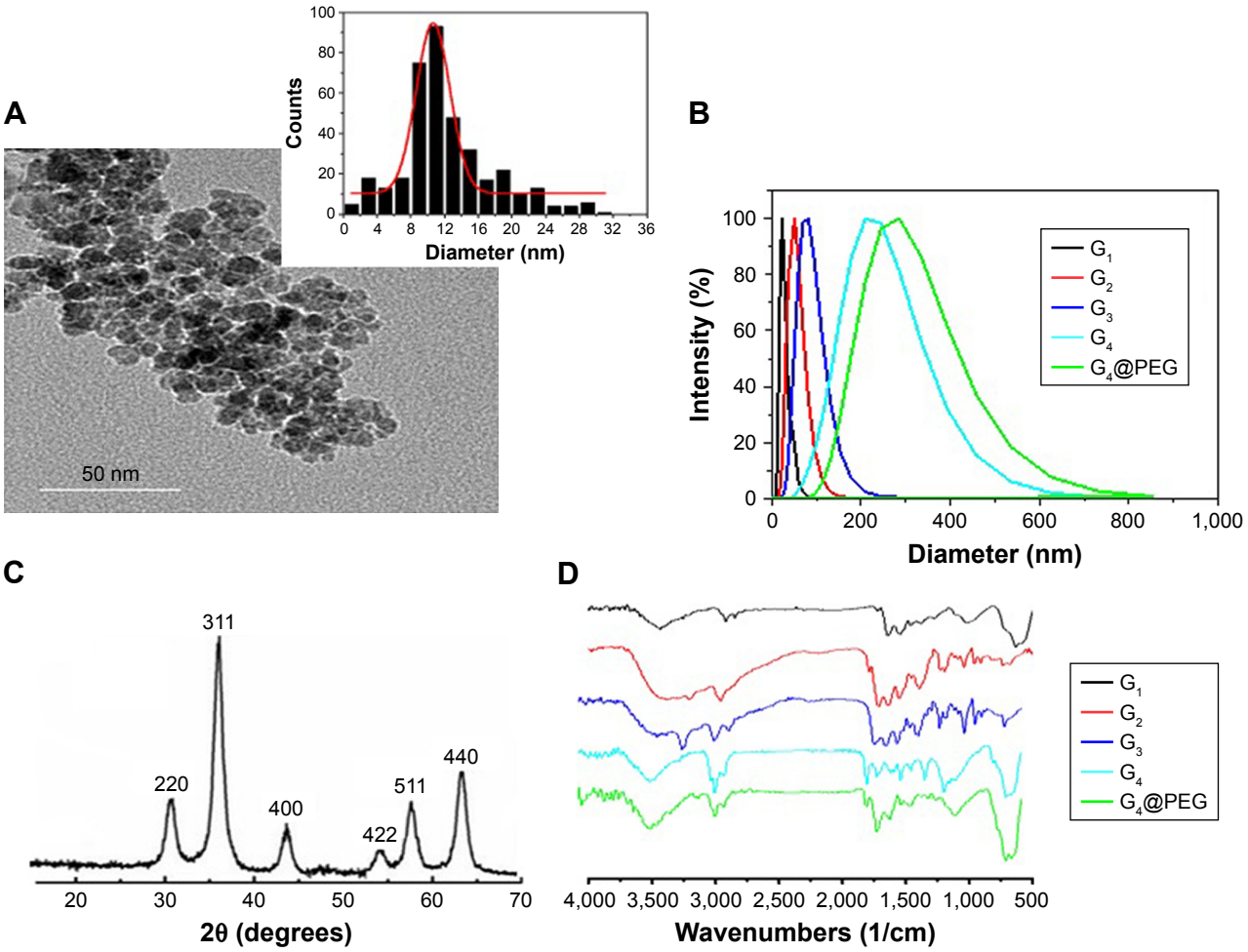

Figure 1 (**A**) TEM image and size distribution of G_4@IONPs. (**B**) DLS shows size distribution and hydrodynamic size of G_1, G_2, G_3, G_4, G_4@PEG@IONPs, (**C**) XRD result identified the crystal structure and all diffraction peaks assigned to Fe_3O_4, and (**D**) FTIR spectra of IONPs coated by G_1, G_2, G_3, G_4, G_4@PEG.
Abbreviations: TEM, transmission electron microscopy; IONPs, iron oxide nanoparticles; DLS, dynamic light scattering; XRD, x-ray diffraction; FTIR, fourier transform infrared spectroscopy.

Histological analysis of kidney and liver

To obtain an accurate evaluation of G_4@IONPs toxicity at the microscopic level, histological staining of kidney and liver tissues was performed (Figure 3). The histopathological results showed edema and losing cytoplasm in the liver cells at 10 mg/kg. There were no significant histopathological variations in the kidney cells in all mice. At doses of 5, 1, and 0.5 mg/kg, no histological abnormalities were detected.

Apoptosis in cardiac tissue

Based on chronic toxicity results, we found out that lactate dehydrogenase (LDH) was elevated at concentrations of 10 and 5 mg/kg. Since this could be a sign of heart injury, TUNEL staining was performed to assess the cardiac toxicity of G_4@IONPs more precisely. The outcomes revealed that apoptosis significantly increased at these concentrations (Figure 4A–E). Also, the quantity (%) of apoptotic cells were 73% and 52% at concentrations of 10 and 5 mg/kg, respectively, compared to 21% in the sham group (Figure 4F). The TUNEL results thereby confirmed blood chemistry outcomes.

Table 1 The hydrodynamic size of coated IONPs by G_1, G_2, G_3, G_4, and G_4@PEG, and their polydispersity percentages

IONPs coated by	G_1	G_2	G_3	G_4	G_4@PEG
Size (nm)	25	53.3	83.7	241.9	298.4
% polydispersity	28	32	31.6	34	31.46

Abbreviation: IONPs, iron oxide nanoparticles.

Biokinetics, tissue distribution, and hemostability of G_4@IONPs

Blood concentration of G_4@IONPs in different time points after IP injection into mice is shown in Figure 5A. The blood iron levels persisted and increased slightly up to 4 h (2.72 ppm) and then decreased to a lower level of 1.57 ppm until 8 h. Finally, at the end of 24 h, the iron concentration decreased to almost half of the maximum amount detected at

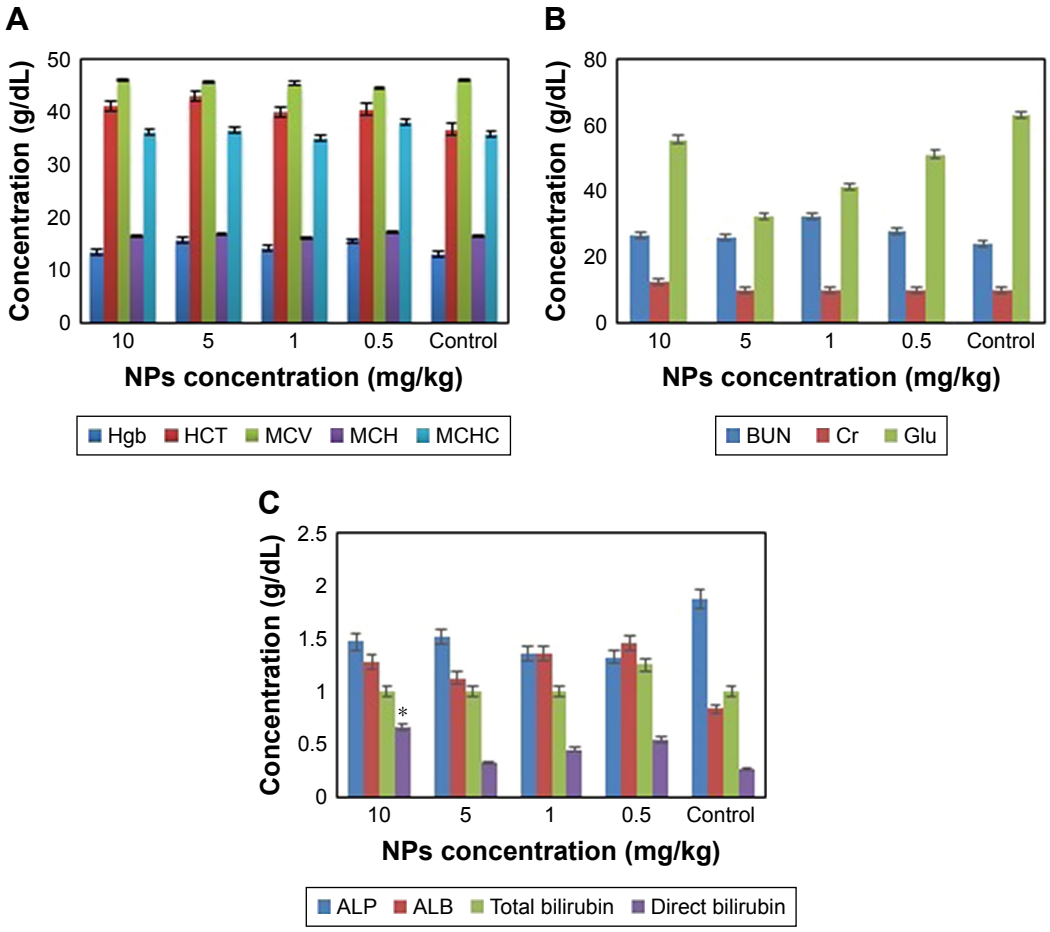

Figure 2 Blood chemistry of (**A**) blood factors, (**B**) renal factors, and (**C**) hepatic factors of animals treated with 10, 5, 1, 0.5, and 0 (control) mg/kg of G_4@IONPs. No significant difference was observed in blood and renal parameters. A significant increase of direct bilirubin was detected in a group of 10 mg/kg (*$P<0.05$).
Abbreviations: IONPs, iron oxide nanoparticles; Hgb, hemoglobin; HCT, hematocrit; MCV, mean corpuscular volume; MCH, mean corpuscular hemoglobin; MCHC, mean corpuscular hemoglobin concentration; BUN, blood urea nitrogen; Cr, creatine; Glu, glucose; ALP, alkaline phosphatase; ALB, albumin; NPs, nanoparticles.

4 h (1.61 ppm). In control mice, 1.2 ppm iron was detected (without any iron injection).

To investigate the tissue distribution and disposition of G_4@IONPs, the concentration of iron in lung, liver, brain, heart, tumor, and kidney tissues at 4, 8, 12, and 24 h after IP injection was determined by the ICP-MS method (Figure 5B).

After administration of a single dose of 5 mg/kg, the iron content was higher in the kidney, liver, and lung. The level

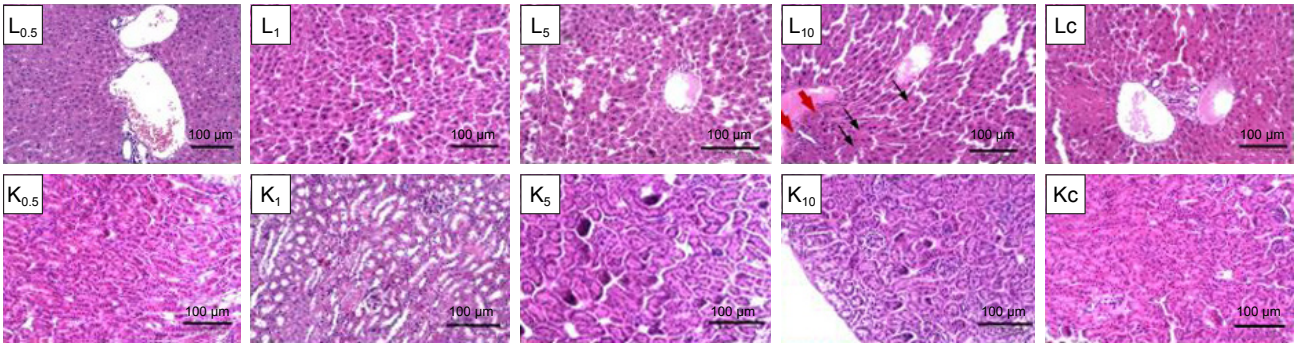

Figure 3 The histopathology images of the liver and kidney; the mice received 10, 5, 1, 0.5, and 0 (control) mg/kg of G_4@IONPs.
Note: Black arrows: edema, red arrows: cytoplasm losing.
Abbreviations: IONPs, iron oxide nanoparticles; L, liver; K, kidney; C, control.

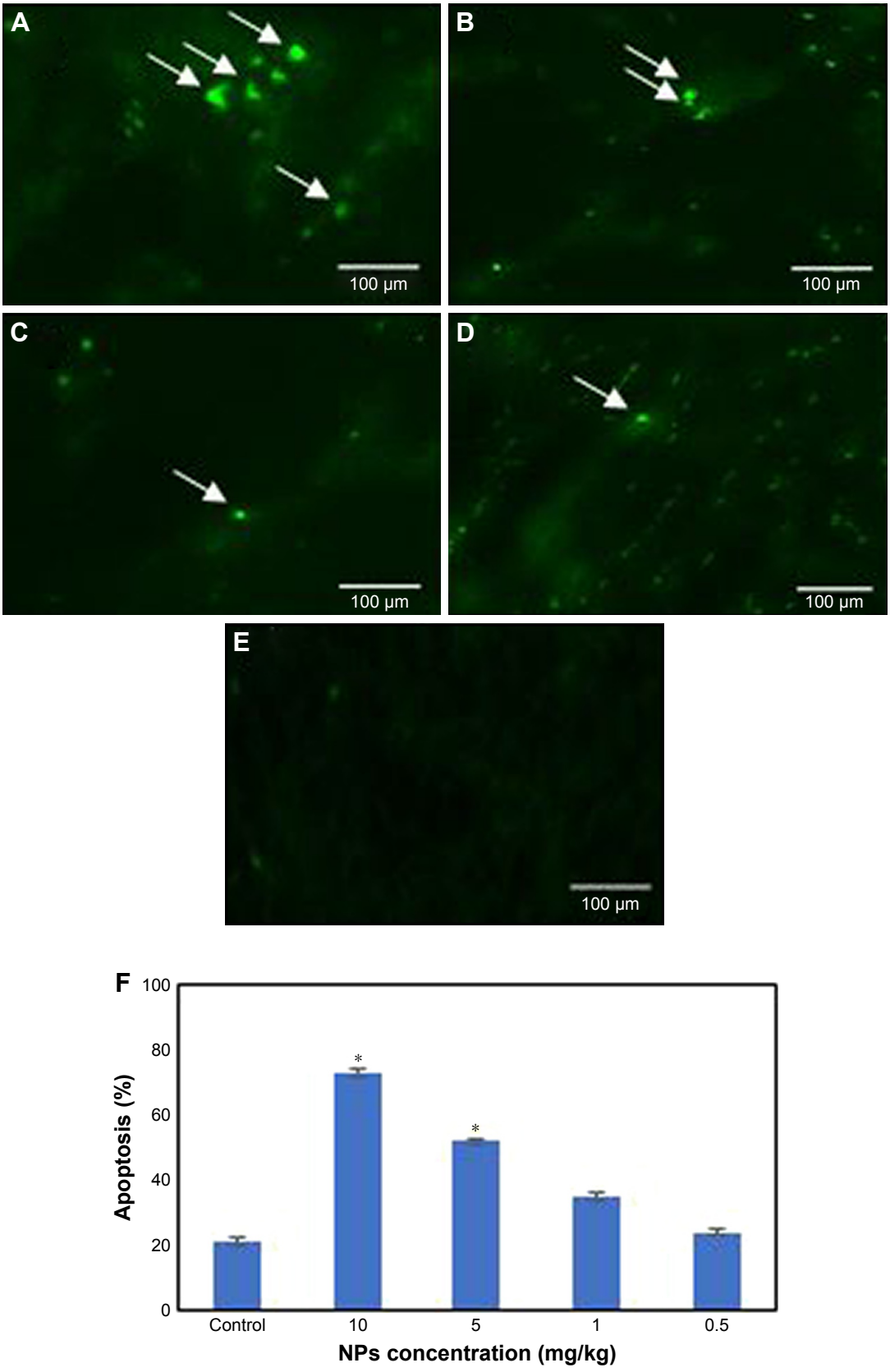

Figure 4 TUNEL staining showed apoptotic cells in cardiac tissue at different G_4@IONPs concentrations (*$P<0.05$): (**A**) 10 mg/kg, (**B**) 5 mg/kg, (**C**) 1 mg/kg, (**D**) 0.5 mg/kg, and (**E**) control. (**F**) TUNEL assay represented the number of apoptotic cells (%) in cardiac tissue (white arrows show the apoptotic cells).
Abbreviations: TUNEL, transferase-mediated dUTP nick end-labeling; IONPs, iron oxide nanoparticles; NPs, nanoparticles.

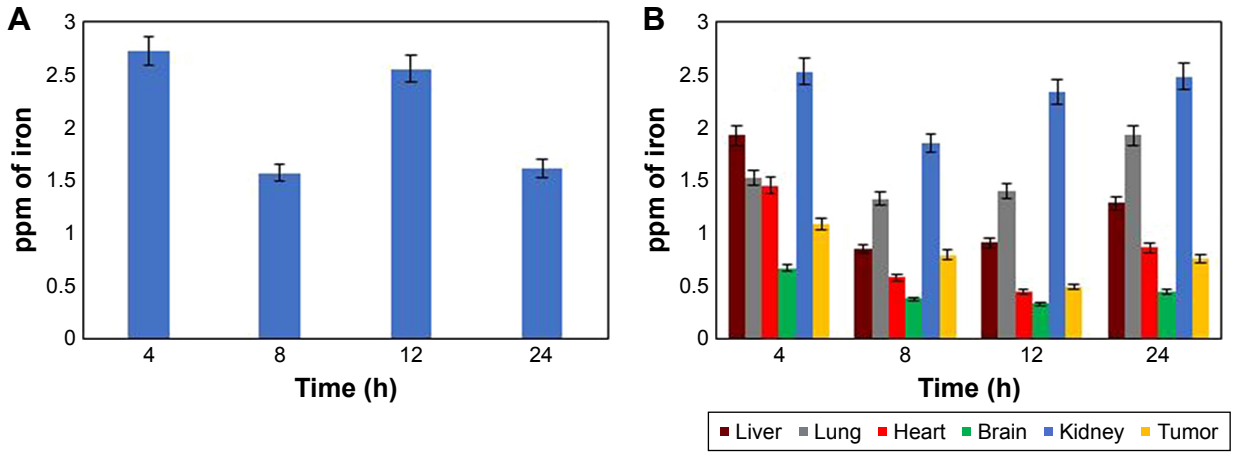

Figure 5 The distribution of G_4@IONPs following IP injection in mice, the concentrations of iron in (**A**) blood and (**B**) lungs, liver, brain, heart, tumor, and kidneys at different time points were determined by ICP-MS.
Abbreviations: IONPs, iron oxide nanoparticles; IP, intraperitoneal; ICP-MS, inductively coupled plasma mass spectrometry; ppm, parts per million.

of iron in the brain remained steady for the entire duration of the experiment (0.45 ppm). In the liver, 1.92 ppm of iron was detected during the first 4 h, then a severe decreasing trend was observed after 8 h (0.84 ppm); finally, 1.27 ppm of iron was detected in the liver, which was almost half of that detected in kidney tissue at this time point (2.47 ppm). It seemed that G_4@IONPs due to their minute size were mostly excreted by kidneys and were finally absorbed in lung tissue. In the lung, the results showed a steady state in iron level during the experimental time, with an increase at 24 h (1.92 ppm). Also, in the tumor tissue, iron content decreased with time; after 4 h, 1.07 ppm of iron was detected in this tissue, while it was just 0.75 ppm after 24 h.

Discussion

Nowadays, dendrimers have attracted a great deal of attention, especially in drug delivery and imaging. It is, therefore, vital to assess their toxicity and biodistribution.[20,31–33] In this study, the G_4@IONPs were synthesized by co-precipitation and coated with G_4 PAMAM dendrimer in a stepwise manner. The results of DLS showed that, by adding each generation of coating layer, the hydrodynamic size of NPs increased. The hydrodynamic diameter was notably larger than the size measured by TEM; that might be due to two main reasons; the scattering of small particles varies strongly with particle radius in DLS, and the signal of larger particles can still overwhelm the signal of smaller ones.

The main disadvantage of DLS is the difficulty in data interpretation of polydispersity with wide particle size distribution. Bigger particles contribute to increasing the light scattering and shifting the measured size toward larger values.[34,35] The polydispersity of G_4@IONPs as measured by TEM and DLS was approximately 32%. In this situation, the enlargement of size distributions induces an error in DLS sizing measurements: sizes are shifted to higher values compared with TEM analyses.[36] The second reason is that the techniques based on light scattering like DLS require a higher concentration of NPs solution, which is more likely to lead to aggregation. Consequently, the aggregated NPs have a disproportionate influence on the analytical signal.[37]

The synthesis procedure of IONPs is greatly influenced by many factors, such as time, temperature, and solution pH, which must, therefore, be carefully controlled.[38,39] These parameters and their effects on synthesized IONPs are listed in Table 2.[40–44] In this study, we synthesized IONPs through a fast method, which took approximately 5 min to complete and did not require heating, which simplified the synthesis process.

To obtain exhaustive information on in vivo G_4@IONPs toxicity, blood chemistry and histological studies were performed. The results showed no significant histological abnormality in the hepatic and renal tissue; while, at concentration

Table 2 The effect of most crucial parameters in IONPs synthesis. The effect of an increase of these parameters (in an optimum range) was shown on bare IONPs characteristics

Initial parameters	Effect			
	Saturation magnetization	Average size	Size distribution	Purity
Ferric (Fe^{+3}) concentration	Increase[40]	Increase[40]	–	–
Time	Increase[41]	Increase[42]	Increase[42]	–
Temperature	Increase[43]	Increase[42]	Decrease[43]	–
pH	Decrease[43]	Increase[43]	–	Increase[44]

Abbreviation: IONPs, iron oxide nanoparticles.

of 10 mg/kg, edema and losing cytoplasm were seen in the liver cells, which might be the result of an accumulation of G_4@IONPs in the liver during 4 h after injection (1.92 ppm); furthermore, indirect bilirubin and BUN levels significantly increased at 10 mg/kg and 100 mg/kg, respectively. IONPs have been reported to be toxic at 60 mg/kg of body mass, while in our study the toxicity level of G_4@IONPs was decreased (100 mg/kg), possibly due to dendrimer coating.[45] IONPs are generally assumed to be biocompatible and non-toxic materials, as their LD_{50} (the dose needed to kill half of the tested animals during a specified time) was reported to be 200–600 mg Fe/kg body weight, while this value increased to 2,000–6,000 mg Fe/kg for dextran-coated IONPs.[46]

Our results showed good agreement with outcomes of other studies; as Jain et al[12] assessed the toxicity of Pluronic coated IONPs with a hydrodynamic size of 186–206 nm in rats, by checking ALT, aspartate aminotransferase and ALP in serum after injection. Also, the amount of lipid hydroperoxide in different tissues was used to analyze the levels of their oxidative stresses due to the administration of the IONPs. They showed that the IONPs only caused minor transient changes, over a period of 6–24 h in the liver enzyme levels. Oxidative stress levels in different tissues also declined after 3 days. These results were also confirmed by histological analyses of the organs, which showed no apparent abnormal changes. In another study, Gu et al[16] studied the in vivo toxicity of the monodisperse oleic acid capped IONPs with a size of 5, 15, and 30 nm, coated with a layer of phospholipid–PEG copolymer. One day after injection, the hematology results revealed an increase in the number of neutrophils which returned back to normal during the next 30 days. This was recognized as the host body defense response to the presence of IONPs. All the other parameters were without any change.

We also assessed the toxicity of G_4@IONPs in cardiac muscle by TUNEL assay, because of the following reasons; an increase of LDH in the blood test, accumulation of a high amount of G_4@IONPs in this tissue, and application of dendrimers in cardiovascular imaging.[32,47] The results indicated that G_4@IONPs could increase apoptosis at concentrations of 5 and 10 mg/kg.

Furthermore, no major change was noted in mice weight and mortality during the experiment time, similar to the other studies. For example, Malik et al[48] found that three daily doses of $G_{3.5}$ PAMAM (95 mg/kg) injected into C_{57} mice bearing B16F10 tumors had no adverse weight changing. In another study, no toxicity or mortality was seen when a single dose (up to 2.56 g/kg) of PEGylated melamine dendrimer was injected into male C3H mice. Also, BUN levels or transaminases remained unchanged.[49]

For biodistribution investigation, the concentration of G_4@IONPs in different tissues was measured during 24 h. At this time point, the maximum amount of G_4@IONPs accumulated in the lung and kidney tissues. It is worth mentioning that the most favorite excretion route for IONPs from the body is through the kidneys, which have negligible intracellular catabolism, so the probability of reactive oxygen species generation is low.[2] Barry[50] claimed that IONPs smaller than 50 nm evade opsonization and are then slowly collected by macrophages in RES; while in our study G_4@IONPs were mainly taken up by the kidney tissue.

The results showed a decrease in accumulated G_4@IONPs in all tissues 8 h after injection. The iron levels at this time declined to approximately half of the primary concentration, except the lung tissue, in which this decrease was only 14%. This might be due to a return of absorbed G_4@IONPs to the bloodstream and then to the spleen or lymph nodes, while the inherent immune system in lungs acts as the main barrier against G_4@IONPs and prevents them from returning to the bloodstream and other organs.[51]

The iron level detected in blood was highest 4 h after injection, while after 8 h this amount decreased. This might be because of accumulation of G_4@IONPs inside the tissues. As mentioned before, at this time, also the amount of iron decreased in tissues so there was just a hypothesis that G_4@IONPs was taken up by other tissues such as lymph nodes or the spleen. After 12 h, the amount of iron increased again and then, at the end of 24 h, this value reached approximately half of the primary amount (1.6 ppm).

Limitations

There were some limitations in our study; first, the experiment duration to determine the biodistribution could have been longer than 24 h. In most tissues, a steady decline in G_4@IONPs concentration was seen, so a longer duration might be necessary to study longer tissue distribution. Second, we did not measure the iron content in the spleen and lymph nodes, which are important organs in RES. Further research could elaborate on the biodistribution of the other generations of dendrimers.

Conclusion

IONPs are gradually being assessed for their potential in targeted drug delivery, magnetic hyperthermia, gene delivery, and as a contrast agent in MRI. A comprehensive clarification of their toxicity and clearance platform seems to be

essential. This study indicated that dendrimers could be an appropriate coating for IONPs, due to their unique properties, such as acceptable toxicity, clearance pattern, and also long circulation time in the BALB/c mice. Obviously, there is a high demand to assess the toxicity and biokinetics of coated IONPs with the other dendrimer generations.

Acknowledgment

This research was supported by a grant from Tehran University of Medical Sciences (grant no. 28169).

Disclosure

The authors report no conflicts of interest in this work.

References

1. Ghalandarlaki N, Alizadeh AM, Ashkani-Esfahani S. Nanotechnology-applied curcumin for different diseases therapy. *BioMed Res Int*. 2014; 2014:394264.
2. Wahajuddin SA. Superparamagnetic iron oxide nanoparticles: magnetic nanoplatforms as drug carriers. *Int J Nanomedicine*. 2012;7: 3445–3471.
3. Chouly C, Pouliquen D, Lucet I, Jeune JJ, Jallet P. Development of superparamagnetic nanoparticles for MRI: effect of particle size, charge and surface nature on biodistribution. *J Microencapsul*. 1996; 13:245–255.
4. Almeida JP, Chen AL, Foster A, Drezek R. In vivo biodistribution of nanoparticles. *Nanomedicine*. 2011;6:815–835.
5. Arami H, Khandhar A, Liggitt D, Krishnan KM. In vivo delivery, pharmacokinetics, biodistribution and toxicity of iron oxide nanoparticles. *Chem Soc Rev*. 2015;44:8576–8607.
6. Weissleder R, Stark DD, Engelstad BL, et al. Superparamagnetic iron oxide: pharmacokinetics and toxicity. *AJR Am J Roentgenol*. 1989;152: 167–173.
7. He C, Hu Y, Yin L, Tang C, Yin C. Effects of particle size and surface charge on cellular uptake and biodistribution of polymeric nanoparticles. *Biomaterials*. 2010;31:3657–3666.
8. Chung TH, Wu SH, Yao M, et al. The effect of surface charge on the uptake and biological function of mesoporous silica nanoparticles in 3T3-L1 cells and human mesenchymal stem cells. *Biomaterials*. 2007;28: 2959–2966.
9. Daniel MC, Tsvetkova IB, Quinkert ZT, et al. Role of surface charge density in nanoparticle-templated assembly of bromovirus protein cages. *ACS Nano*. 2010;4:3853–3860.
10. Papisov MI, Bogdanov A, Schaffer B, et al. Colloidal magnetic resonance contrast agents: effect of particle surface on biodistribution. *J Magn Magn Mater*. 1993;122:383–386.
11. Xiao K, Li Y, Luo J, et al. The effect of surface charge on in vivo biodistribution of PEG-oligocholic acid based micellar nanoparticles. *Biomaterials*. 2011;32:3435–3446.
12. Jain TK, Reddy MK, Morales MA, Leslie-Pelecky DL, Labhasetwar V. Biodistribution, clearance, and biocompatibility of iron oxide magnetic nanoparticles in rats. *Mol Pharm*. 2008;5:316–327.
13. Cole AJ, David AE, Wang J, Galbán CJ, Hill HL, Yang VC. Polyethylene glycol modified, cross-linked starch-coated iron oxide nanoparticles for enhanced magnetic tumor targeting. *Biomaterials*. 2011;32: 2183–2193.
14. Chandra S, Nigam S, Bahadur D. Combining unique properties of dendrimers and magnetic nanoparticles towards cancer theranostics. *J Biomed Nanotechnol*. 2014;10:32–49.
15. Opina AC, Wong KJ, Griffiths GL, et al. Preparation and long-term biodistribution studies of a PAMAM dendrimer G5–Gd-BnDOTA conjugate for lymphatic imaging. *Nanomedicine*. 2015;10:1423–1437.
16. Gu L, Fang RH, Sailor MJ, Park JH. In vivo clearance and toxicity of monodisperse iron oxide nanocrystals. *ACS Nano*. 2012;6: 4947–4954.
17. Tajabadi M, Khosroshahi ME, Bonakdar S. An efficient method of SPION synthesis coated with third generation PAMAM dendrimer. *Coll Surf A*. 2013;431:18–26.
18. Khodadust R, Unsoy G, Yalcın S, Gunduz G, Gunduz U. PAMAM dendrimer-coated iron oxide nanoparticles: synthesis and characterization of different generations. *J Nanopart Res*. 2013;15: 1488.
19. Kojima C, Turkbey B, Ogawa M, et al. Dendrimer-based MRI contrast agents: the effects of PEGylation on relaxivity and pharmacokinetics. *Nanomedicine*. 2011;7:1001–1008.
20. Longmire M, Choyke PL, Kobayashi H. Dendrimer-based contrast agents for molecular imaging. *Curr Top Med Chem*. 2008;8: 1180–1186.
21. Farhangi B, Alizadeh AM, Khodayari H, et al. Protective effects of dendrosomal curcumin on an animal metastatic breast tumor. *Eur J Pharmacol*. 2015;758:188–196.
22. Mehravi B, Alizadeh AM, Khodayari S, et al. Acute toxicity evaluation of glycosylated Gd3+-based silica nanoprobe. *Mol Imaging Biol*. 2017; 19:522–530.
23. Xue Y, Zhang S, Huang Y, et al. Acute toxic effects and gender-related biokinetics of silver nanoparticles following an intravenous injection in mice. *J Appl Toxicol*. 2012;32:890–899.
24. Arama E, Steller H. Detection of apoptosis by terminal deoxynucleotidyl transferase-mediated dUTP nick-end labeling and acridine orange in Drosophila embryos and adult male gonads. *Nat Protoc*. 2006;1: 1725–1731.
25. Roca AG, Costo R, Rebolledo AF, et al. Progress in the preparation of magnetic nanoparticles for applications in biomedicine. *J Phys D Appl Phys*. 2009;42:224002.
26. Spizzo F, Sgarbossa P, Sieni E, et al. Synthesis of ferrofluids made of iron oxide nanoflowers: Interplay between carrier fluid and magnetic properties. *Nanomaterials*. 2017;7:E373.
27. Langford JI, Wilson AJC. Scherrer after sixty years: a survey and some new results in the determination of crystallite size. *J Appl Crystallogr*. 1978;11:102–113.
28. Julian J, Anderson D, Brandau A, et al. *An Infrared Spectroscopy Atlas for the Coatings Industry*. Blue Bell, PA: Federation of Societies for Coatings Technology; 1991.
29. Yamaura M, Camilo RL, Sampaio LC, Macêdo MA, Nakamura M, Toma HE. Preparation and characterization of (3-aminopropyl) triethoxysilane-coated magnetite nanoparticles. *J Magn Magn Mater*. 2004;279:210–217.
30. Tsubokawa N, Takayama T. Surface modification of chitosan powder by grafting of 'dendrimer-like' hyperbranched polymer onto the surface. *React Funct Polym*. 2000;43:341–350.
31. Myc A, Kukowska-Latallo J, Cao P, et al. Targeting the efficacy of a dendrimer-based nanotherapeutic in heterogeneous xenograft tumors in vivo. *Anticancer Drugs*. 2010;21:186–192.
32. Seo JW, Baek H, Mahakian LM, et al. 64Cu-labeled LyP-1-dendrimer for PET-CT imaging of atherosclerotic plaque. *Bioconjug Chem*. 2014; 25:231–239.
33. Wang SJ, Brechbiel M, Wiener EC. Characteristics of a new MRI contrast agent prepared from polypropyleneimine dendrimers, generation 2. *Invest Radiol*. 2003;38:662–668.
34. Rigler R, Elson ES. *Fluorescence Correlation Spectroscopy: Theory and Applications*: Berlin, Germany: Springer Science & Business Media; 2012.
35. Kim HA, Seo JK, Kim T, Lee BT. Nanometrology and its perspectives in environmental research. *Environ Health Toxicol*. 2014;29: e2014016.

36. Souza TGF, Ciminelli VST, Mohallem NDS. A comparison of TEM and DLS methods to characterize size distribution of ceramic nanoparticles. *J Phys Conf Series*. 2016;733:012039.
37. Domingos RF, Baalousha MA, Ju-Nam Y, et al. Characterizing manufactured nanoparticles in the environment: multimethod determination of particle sizes. *Environ Sci Technol*. 2009;43:7277–7284.
38. Ali A, Zafar H, Zia M, et al. Synthesis, characterization, applications, and challenges of iron oxide nanoparticles. *Nanotechnol Sci Appl*. 2016; 9:49–67.
39. Mamani JB, Gamarra LF, Brito GEDS. Synthesis and characterization of Fe_3O_4 nanoparticles with perspectives in biomedical applications. *Mater Res*. 2014;17:542–549.
40. Vega-Chacón J, Picasso G, Avilés-Félix L, Jafelicci M. Influence of synthesis experimental parameters on the formation of magnetite nanoparticles prepared by polyol method. *Adv Nat Sci Nanosci Nanotechnol*. 2016;7:015014.
41. Prem Ananth K, Jose SP, Venkatesh KS, Ilangovan R. Size controlled synthesis of magnetite nanoparticles using microwave irradiation method. *J Nano Res*. 2013;24:184–193.
42. Petcharoen K, Sirivat A. Synthesis and characterization of magnetite nanoparticles via the chemical co-precipitation method. *Mater Sci Eng B*. 2012;177:421–427.
43. Tajabadi M, Khosroshahi ME. Effect of alkaline media concentration and modification of temperature on magnetite synthesis method using $FeSO_4/NH_4OH$. *Int J Chem Eng Applic*. 2012;3:206–210.
44. Faiyas APA, Vinod EM, Joseph J, Ganesan R, Pandey RK. Dependence of pH and surfactant effect in the synthesis of magnetite (Fe_3O_4) nanoparticles and its properties. *J Magn Magn Mater*. 2010;322:400–404.
45. Goldhaber SB. Trace element risk assessment: essentiality vs. toxicity. *Regul Toxicol Pharmacol*. 2003;38:232–242.
46. Wada S, Yue L, Tazawa K, et al. New local hyperthermia using dextran magnetite complex (DM) for oral cavity: experimental study in normal hamster tongue. *Oral Dis*. 2001;7:192–195.
47. Liu H, Wang H, Xu Y, et al. Synthesis of PEGylated low generation dendrimer-entrapped gold nanoparticles for CT imaging applications. *Nanoscale*. 2014;6:4521–4526.
48. Malik N, Evagorou EG, Duncan R. Dendrimer-platinate: a novel approach to cancer chemotherapy. *Anticancer Drugs*. 1999;10:767–776.
49. Chen HT, Neerman MF, Parrish AR, Simanek EE. Cytotoxicity, hemolysis, and acute in vivo toxicity of dendrimers based on melamine, candidate vehicles for drug delivery. *J Am Chem Soc*. 2004;126: 10044–10048.
50. Barry SE. Challenges in the development of magnetic particles for therapeutic applications. *Int J Hyperthermia*. 2008;24:451–466.
51. Al Faraj A, Shaik AP, Shaik AS. Effect of surface coating on the biocompatibility and in vivo MRI detection of iron oxide nanoparticles after intrapulmonary administration. *Nanotoxicology*. 2015;9:825–834.